TURBULENT FORCE FLOW IN AN AIRBLAST STORAC

Li Chen and Yuguo Li

Advanced Thermo-fluids Technologies Laboratory
CSIRO Building, Construction and Engineering, Melbourne, AUSTRALIA

ABSTRACT

Forced air circulation in a storage room either with freezing/cooling or controlled atmosphere is usually turbulent because a high air change rate is generally required. The interaction between the turbulent air flow and the product layers plays an important role in the performance of the storage room. In this paper, a homogenous model based on the Brinkman–Forchheimer-extended Darcy equation for both fluid and porous layer is described, in association with the standard k–ε turbulence model. Turbulent forced air circulation in a room containing porous layers is studied numerically by this model. A second-order control volume technique is used for the discretisation of the governing equations. SIMPLEC is adopted for the treatment of the pressure–velocity coupling. The predicted results are compared with available experimental results in the literature. The effects of two different stored products on the flow field in the product layers are investigated, and useful information is provided for the optimised design of a storage room.

KEYWORDS

Air exchange efficiency, air velocity, CFD, modelling, porous medium.

INTRODUCTION

There are many types of storage enclosures where the stored products can be modelled as porous media, such as containers for transport of perishable commodities, foods and banana ripening cool rooms or controlled atmosphere rooms. One aim in designing these storage enclosures is to ensure a uniform targeted temperature or specie distribution in the stored products. Heat and mass transfer in stored product layers becomes very important in maintaining good quality stored products, which is mainly dependent of the interaction between the supply air flow and the product structures. Both the complex transport mechanics and the complex geometry of a storage room and its product layers present challenges to any theoretical and experimental investigation.

This study concerns mainly the influence of the turbulent flows on the micro-environment of stored products in a controlled atmosphere storage room. However, the methodologies developed are also applicable to other types of storage rooms.

There have been many fundamental studies of transport mechanics in porous media, e.g. Beaver and Joseph *et al.* (1967), Vafai and Tien (1981), Hsu and Cheng (1991), Nield (1991), Vafai and Kim (1995) and Ochoa–Tapia and Whitaker (1995). In general, the flow models used in these studies are based on either Darcy's law or its extension. In particular, the Brinkman–Forchheimer-extended Darcy (BFD) equation (Hsu and Cheng 1991) has been widely used, possibly due to its similarity to the Navier–Stokes equations.

Beckermann *et al.* (1988) studied both experimentally and numerically the natural convection flows at low Rayleigh numbers in an enclosure partially filled with a porous medium using the non-Darcian model incorporating Brinkman and Forchheimer extensions. In their model, the equations for the porous layer and the Navier–Stokes equation for the fluid region are linked by an indicator function. In contrast, in an investigation (Chen and Chen 1992) of the laminar natural convection in a partially filled enclosure heated from below, the fluid and porous layers were solved separately, and continuous interfacial conditions had to be applied at the fluid–porous interface.

It seems that most previous studies are associated with laminar flows in the fluid region. Song and Viskanta (1994) used the model developed by Hsu and Cheng (1991) to study high Rayleigh number natural convection in an enclosure partly filled with a porous medium. Very recently, Antohe and Lage (1997) developed a generalised k–ε

model for porous media based on the BFD. Their turbulence model for porous media is considered an extension of the standard k–ε turbulence model. However no computational results were presented in their paper.

With regard to storage rooms, Wang and Touber (1990) studied the force convection in a refrigerated room. In their model, the standard k–ε model was adopted to study the turbulent force convection, but interactions between air flow and products were neglected. The flow field inside products was obtained by a simplified Bernoulli equation. Fong (1996) measured flow patterns and velocity profiles in a controlled atmosphere storage room. A commercial CFD program, FIDAP, was used to simulate the flow field and nitrogen dispersion in the storage room. Tanka and Xin (1997) studied experimentally the effects of the structure and stacking configuration of containers for the transport of chicks and found that the influence on heat transfer in the chicks was significant.

In this paper, a homogenous model based on Hsu and Cheng (1991) for both fluid and porous regions is described, together with the extended standard k–ε turbulence model of Antohe and Lage (1997). Because a volume fraction of the clear fluid relative to the porous medium is introduced, there is no need to specify the matching conditions at the fluid–porous medium interface. This enables us to solve the whole computational domain with only one set of equations and to understand the details of the interferences between turbulent air flow and stored products.

PROBLEM FORMULATION

Consider a controlled atmosphere room (Fong 1996) containing three layers of products, as shown in Figure 1. The side walls, floor and ceiling are adiabatic. The air is supplied at a constant velocity and temperature. The configuration was chosen to match the experimental rig used by Fong (1996). With a stack structure of products, only the top lid is permeable, which may not be realistic in practice but is chosen here to reproduce the same test geometry as in the experimental study of Fong (1996).

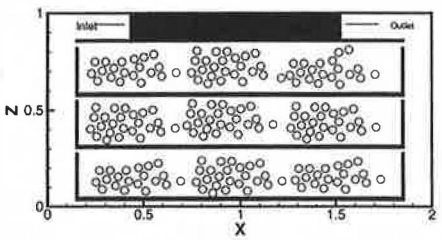

Figure 1 Schematic of controlled atmosphere storage room.

Following Hsu and Cheng (1991), the macroscopic conservation of mass, momentum and energy of the flow in the porous medium can be described by the extended Navier–Stokes equations with the BFD model. According to Chen and Chen (1992), continuous velocity, temperature and normal shear stresses at the fluid–porous interface result in the pressure being continuous. When the fluid–porous interface coincides with the computational grid, a homogeneous model can be derived in terms of the porosity of a porous medium. The fluid is assumed to be incompressible and to satisfy the Boussinesq approximation. The conservation of mass, momentum and energy can be written as:

$$\frac{\partial \bar{U}_j}{\partial x_j} = 0 \tag{1}$$

$$\frac{\partial}{\partial x_j}(\rho U_i U_j) = -\frac{\partial \bar{p}}{\partial x_i} + (T - T_{ref})g_i + \frac{\partial}{\partial x_j}\left[(\mu_f + \mu_T)\left(\frac{\partial U_i}{\partial x_j} + \frac{\partial U_j}{\partial x_i}\right)\right] - (1 - F^2)B_i \tag{2}$$

$$\frac{\partial}{\partial x_j}(U_i T) = \frac{\partial}{\partial x_j}\left[(\alpha_{eff} + \alpha_T)\frac{\partial T}{\partial x_j}\right] \tag{3}$$

where U_i = time-averaged Darcy velocity tensor
P = time averaged Darcy pressure
T, T_{ref} = time averaged Darcy temperature and temperature of supply air
μ_f = fluid viscosity
ρ = density
g_i = gravity acceleration tensor
F = porosity of porous layer

It should be noted that F is 1 in the fluid region and <1 in the porous region. The other properties are given by:

$$\rho = \frac{\rho_f}{F}, \alpha_{eff} = \frac{k_{eff}}{\rho_f c_{p,f}} = \frac{k_f (k_b/k_f)^{1-F}}{\rho_f c_{p,f}} \quad (4)$$

where c_p is the specific heat.

The effective thermal conduction, k_{eff}, for the porous layer is modelled using the empirical relationship suggested by Beckermann *et al.* (1988). Subscripts, f and b, are for a fluid and pore of a porous medium respectively. The last term in equation (2), which is due to the Darcy and Forchheimer extensions, is given by:

$$B_i = \left[\frac{\mu_f U_i}{K} \mu U_i + \frac{CF\rho_f}{\sqrt{K}} (U_j U_j)^{1/2} U_i \right] \quad (5)$$

where $K = \dfrac{F^3 d^2}{175\,(1-F)^2}$

= permeability of porous layer

$C = \dfrac{175\,(1-F)\sqrt{K}}{F^3 d}$

= the inertial coefficient

d = pore size of the porous medium

The standard k–ε model with the Darcy and Forchheimer terms based on Antohe and Lage (1997) can be written as:

$$\frac{\partial}{\partial x_j}(\rho U_i k) = \left\langle \frac{\partial}{\partial x_j}\left[\left(\mu + \frac{\mu_T}{\sigma_k} \right) \frac{\partial}{\partial x_j} \right] \right\rangle + p_k + G_k - \rho\varepsilon + (1-F^2) B_k \quad (6)$$

$$\frac{\partial}{\partial x_j}(\rho U_i \varepsilon) = \frac{\partial}{\partial x_j}\left[\left(\mu + \frac{\mu_T}{\sigma_k} \right) \frac{\partial \varepsilon}{\partial x_j} \right] + c_{1\varepsilon} f_1 P_k + c_{1\varepsilon} f_1 c_{3\varepsilon} G_k - c_{2\varepsilon} f_2 \rho \frac{\varepsilon}{k} + (1-F^2) B_\varepsilon \quad (7)$$

with

$$P_k = \mu_T \frac{\partial U_i}{\partial x_j}\left(\frac{\partial U_i}{\partial x_j} + \frac{\partial U_j}{\partial x_i} \right),$$

$$G_k = -\rho \alpha_T \frac{\partial \theta}{\partial x_{i2}} \quad (8)$$

In above equations, μ_T and α_T are the turbulent viscosity and thermal diffusivity and are defined by:

$$\mu_T = C_\mu \frac{k^2}{\varepsilon}, \alpha_T = \frac{c_\mu}{\sigma_T} \frac{k^2}{\varepsilon} \quad (9)$$

where k, ε is the turbulent kinetic energy and its dissipation rate.

The basic difference between the new turbulence transport equations and the standard k–ε equations is the two new terms, B_k and B_ε in equations (6) and (7), which are given by:

$$B_k = -\left[\frac{2\mu}{K} + \frac{2C\rho_f F}{\sqrt{K}} (U_j U_j)^{1/2} \right] k \quad (10)$$

$$B_\varepsilon = -\left[\frac{2\mu}{K} + \frac{2C\rho_f F}{\sqrt{K}} (U_j U_j)^{1/2} \right] \varepsilon - \frac{2C\rho_f F}{2(Da)^{1/2}} \mu \frac{\partial (U_j U_j)^{1/2}}{\partial x_r} \frac{\partial k}{\partial x_r} \quad (11)$$

In deriving the k and ε transport equations, a different expansion form from the one used by Antohe and Lage (1997) is used, which gives:

$$\left| U_j + \mu_j' \right| (U_i + \mu_i') \approx (U_j U_j)^{1/2} U_i + (U_j U_j)^{1/2} \mu_j' \quad (12)$$

The new expansion form simplifies the derivation of the turbulence transport equations. It has been found that for the problem of interest, there is little difference in the solutions of the k and ε equations between our formulation (12) and that of Antohe and Lage (1997).

The commonly used wall functions are applied at the first grid points near the boundaries. The boundary conditions for k and ε are defined:

$$y^+ = \frac{\rho u_\tau y}{\mu}, k = \frac{u_\tau^2}{\sqrt{(c_\mu)}}, \varepsilon = \frac{\rho u_\tau^4}{0.41\,\mu y^+} \quad (13)$$

The closure coefficients are:

$$c_\mu = 0.09,\ c_{1\varepsilon} = 1.44,\ c_{2\varepsilon} = 1.92,\ \sigma_T = 1.0$$
$$\sigma_k = 1.0,\ \sigma_\varepsilon = 1.3,\ f_\mu = f_1 = f_2 = 1.0 \quad (14)$$

The $c3$ formulation proposed by Henkes *et al.* (1991) is adopted in this study.

NUMERICAL METHOD

A control volume method on a non-uniform staggered grid, guarantees a higher mesh resolution near all walls and a coarse resolution in the products region, which improves computational efficiency. The diffusion terms are discretised using the centre

differencing scheme; convection terms using the second-order QUICK scheme. The detail of the numerical implementation can be found in Li and Rudman (1995). Pressure–velocity coupling is treated using the SIMPLE algorithm (Patankar 1980). The resulted linear system of equations is solved by TDMA method (Patankar 1980).

RESULTS AND DISCUSSION

To validate the accuracy of the present model, a mesh-independent test and a comparison with available experimental results were carried out with a constant air supply, u_{sup} = 4.37 m/s. All side walls of the layers were impermeable. Following the experiments, the products (polystyrene beans) were homogenously distributed in each layer with a porosity of 0.4 and a pore size of 7×10^{-3} (m). This corresponds to a permeability of 4.98×10^{-8} based on its definition.

The problem was firstly simulated using three different grids ($x \times y$): 45 × 58, 91 × 108 and 181 × 218. The results for the convergence are shown in Figures 2 and 3. It can be seen from Figure 2 that the coarsest mesh (45 × 58) failed to predict the details of some flow features, such as the two vortexes in the right air column. The flow characteristics were nearly identical when the meshes was further doubled from 91 × 108 to 181 × 218.

For a further demonstration of the convergence, the vertical velocity profiles along the x coordinate are plotted at three different heights and shown in Figure 3. The velocity profiles at the middle height of the bottom layer with x ranging from 1.8 to 2 m (the right air column) is shown in Figure 3a, at the middle layer for the left column in Figure 3b and at the top layer for the right column in Figure 3c. It can be seen that the results predicted using the two meshes (91 × 108 and 181 × 218) converged well, but the predicted peak vertical velocities in the right air column using the 91 × 108 mesh is slightly higher than those predicted using the 181 × 218 mesh. The vertical velocities were close to zero in the product layers with all meshes. Thus, the solution obtained using 91 × 108 can be claimed to be nearly mesh-independent, at least for the global flow pattern. This mesh was used for the remaining test described in this paper unless otherwise specified.

Following the grid-independent test, the predicted results with the 91 × 108 mesh were compared against the experimental data (Fong 1996). The flow pattern measured by Fong is shown in Figure 4. The similarity between the predicted and experimental results can be clearly seen in Figures 2b and 4. The comparisons of the predicted vertical velocity profiles against experimental data are shown in Figure 5. The vertical velocity profiles in the right air column were predicted very well, although the peaks are slightly overpredicted. However, significant differences were obtained for the velocity profiles in the left column. This can be attributed to the fact that the experimental rig is very leaky, as Fong (1996) suggested. Giving the measuring and unknown error in experimental work, the agreements between predicted and experimental results are, in general, reasonable good. A better comparison could be achieved by refining the mesh, but this was not carried out due to time limitations.

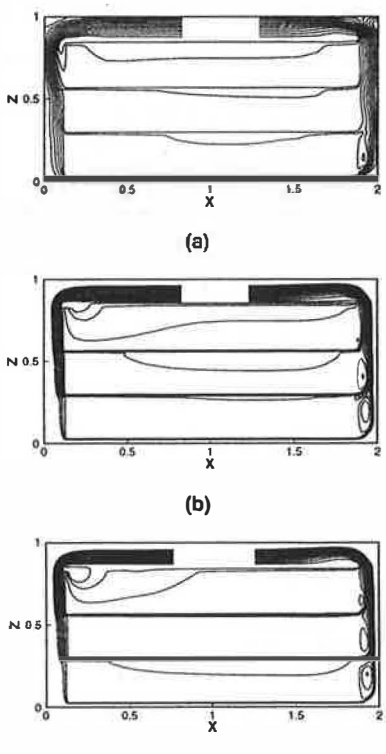

Figure 2 Streamline plots (contour levels 0.2–0.6) with different meshes: (a) 45 × 58, (b) 91 × 108 and (c) 181 × 218).

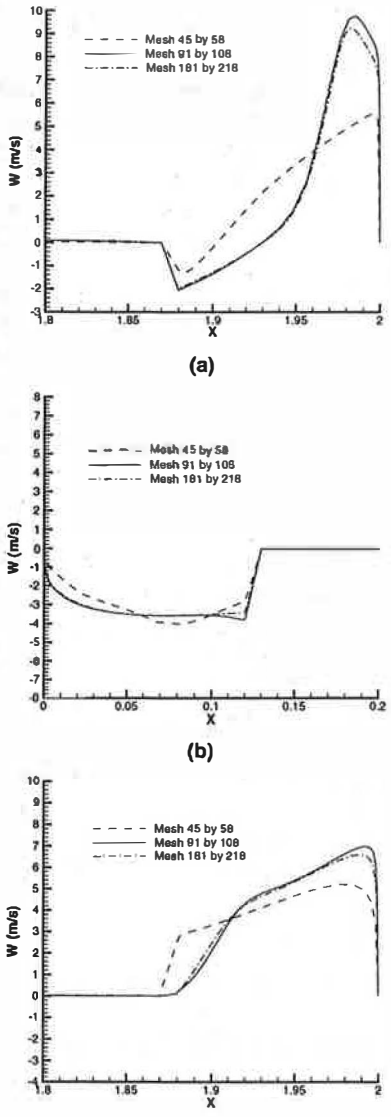

Figure 3 Effect of mesh size on profiles of the vertical component of velocity vector at: (a) z = 0.152 m, (b) z = 0.44 m and (b) z = 0.72 m.

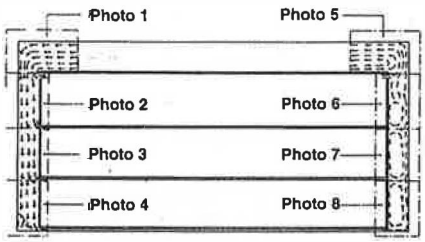

Figure 4 Schematic representation of the flow visualisation results of Fong (1996).

ANALYSIS OF FLOW CHARACTERISTICS IN THE ROOM

The velocity field is shown in Figure 6 which, for clarity, only shows a small number of grid points. High velocities from three horizontal air gaps introduce three air jets into the right air column. The jets impinge to the right wall and bend towards upwards. Vortices are formed between every two jets in the low-pressure regions. Three recirculation regions are formed, with the strongest at the bottom and the weakest at the top. The strongest vortex is formed due to the highest jet velocity issued from the bottom air gap (see Figure 2c). Reasonable grid resolution is required to resolve the three vortices, in particular the smallest one at the top. For the top air gap, the jet velocity is relatively low.

Based on the streamline plot in Figure 2b, it can been seen that the penetration of air into the products is very weak because of high resistance in the product layers. The product layers are acting more or less as rigid walls. The magnitude of the velocity in product layers is much lower than 0.5 m/s, which is about 30 times lower than the average value in a horizontal air gap above the layer (Figure 7). The majority of air flows downwards after it enters the left column. As expected, the lowest layer attracts the highest air flow rate. The flow shows similar distribution patterns in the two lower product layers. In Figure 8, the negative values of the vertical velocity component for the two lower product layers at x = 0.5 imply that air penetration occurs. Air penetration to the upper layer is much weaker than to the other two, and occurs at the very left part of the layer, as may be seen from the streamline in Figure 2.

The distribution of turbulent kinetic energy in the room is shown in Figure 9, where contour levels are plotted from 0.001 to 8 and the lowest values are observed in the product regions. The most intensive turbulence occurs when air enters the three horizontal air gaps. The turbulence in each product region is close to zero except at the left and right corners of each product layer, where air penetration and extraction occur. It should be noted that turbulence is slightly stronger and exists in wider regions in the two lower product layers because of the higher air penetration. For the upper porous layer, the flow is turbulent only in a very thin layer. These results are consistent with the predicted velocity field.

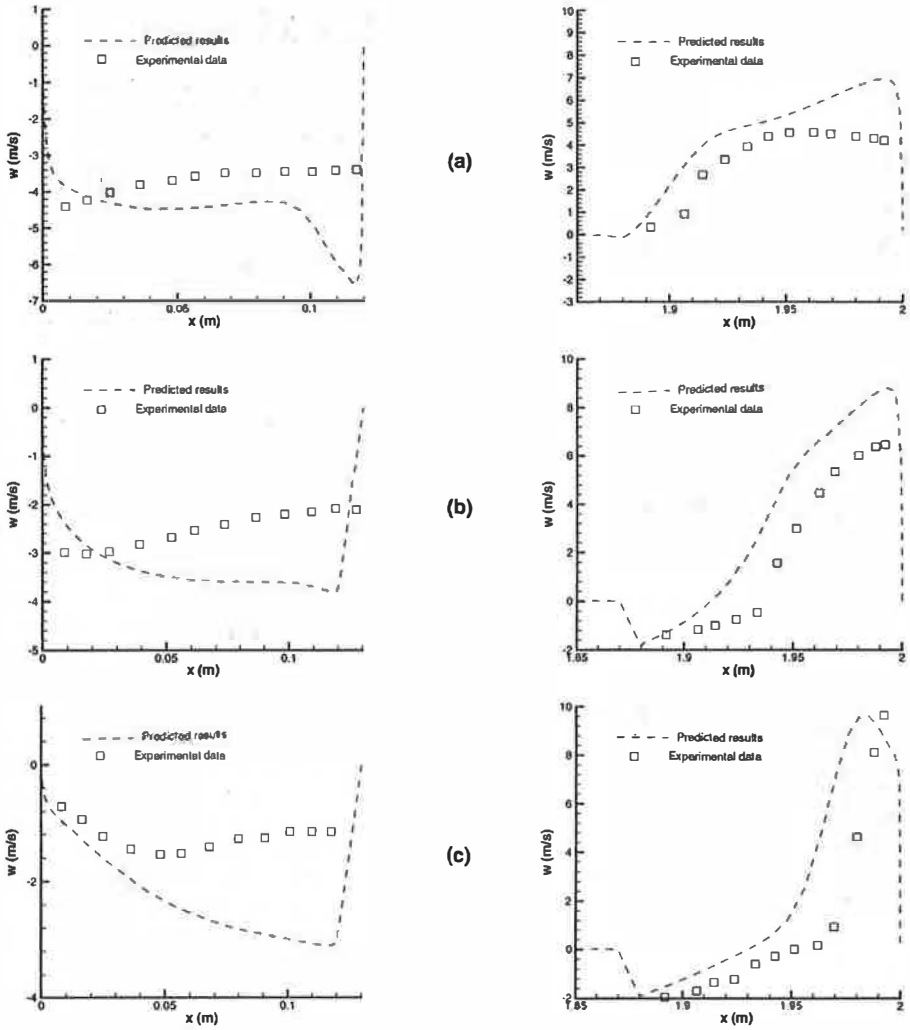

Figure 5 Comparison of predicted and measured distribution of the vertical components of velocity vector at different z plates: (a) $z = 0.72$, (b) $z = 0.42$ and (c) $z = 0.142$.

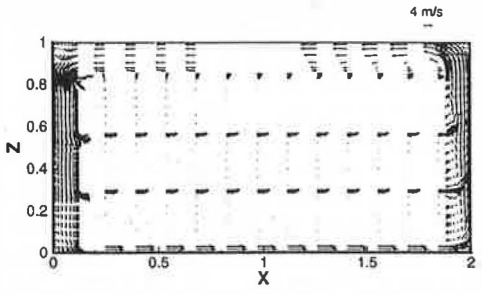

Figure 6 Velocity vector with $u_{sup} = 4.37$ m/s, $d = 7 \times 10^{-3}$ and $F = 0.4$.

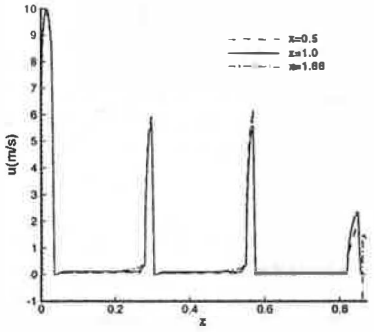

Figure 7 Horizontal velocity component distributions in three product layers at different x plates ($u_{sup} = 4.37$ m/s, $d = 7 \times 10^{-3}$ and $F = 0.4$).

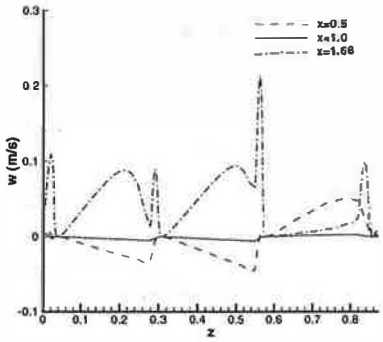

Figure 8 Vertical velocity distributions at different x plates (u_{sup} = 4.37 m/s, $d = 7 \times 10^{-3}$ and $F = 0.4$).

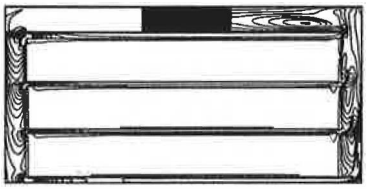

Figure 9 Turbulent kinetic energy contours for beans (levels: 0.001–8).

EFFECT OF PRODUCT PERMEABILITY ON AIR FLOW PATTERN

It is important to understand the influence of the structure of the products on the flow field in its stack region. This can be studied by varying products in the layers, such as changing the products from bean to apple, in which the size of pore and porosity of the product's medium is changed.

In this paper, a case for apple storage is studied. Taking the average apple size as 8×10^{-2} (m) and assuming an ideal packing pattern of the porosity of 0.4767, permeability is equal to 1.45×10^{-5}. The geometry of the room, structure of the stacks and air supply are the same as for the beans.

A comparison of flow patterns in apple and bean storage is shown in Figure 10. The differences are obvious. With a big pore and higher porosity of the medium, i.e. a higher permeability, a lower flow resistance results. The very high velocity air in the horizontal gaps between the product layers drove the circulations of the fluid inside the product layers in the apple storage (Figures 10, 11), rather than penetrating into the products from the left side, as in the bean storage (see Figure 12, in which vertical velocities were always positive). With such a flow feature in

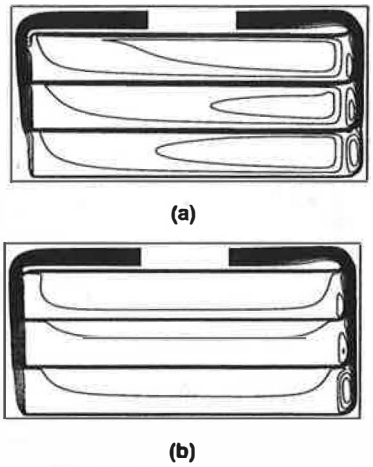

Figure 10 Effect of permeability of products on streamline: (a) $d = 8 \times 10^{-2}$, $F = 0.4767$ and (b) $d = 7 \times 10^{-3}$, $F = 0.4$.

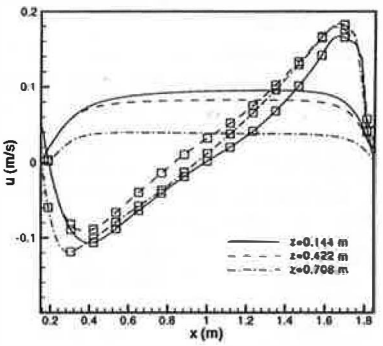

Figure 11 Effect of permeability of products on horizontal component of velocity vector distribution at the middle plate of three product layers (squared lines are for results with high permeability: $d = 8 \times 10^{-2}$, $F = 0.4767$; plain lines are for $d = 7 \times 10^{-3}$, $F = 0.4$.

stored products, energy and mass will be dispersed between air and products by the diffusion and convection through the horizontal air/product interface. It is expected that an increase in permeability resulted in an increase in the maximum air velocity inside the apple storage, which was actually double that in bean storage, as may be seen in Figure 11. As a result, the flow inside the apple storage was more turbulent, and the turbulent region mainly concentrated on the air/apple interface and the right side of the product layers (Figure 13).

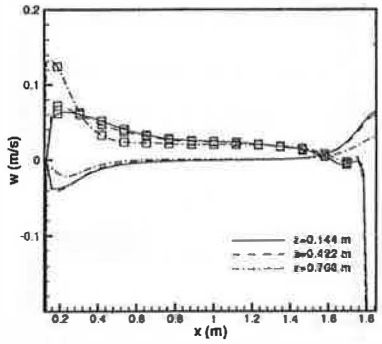

Figure 12 Effect of permeability of products on vertical component of velocity vector distribution at the middle plate of three product layers (squared lines are for results with high permeability: $d = 8 \times 10^{-2}$, $F = 0.4767$; plain lines are for $d = 7 \times 10^{-3}$, $F = 0.4$.

CONCLUSION

Forced ventilation in a cold storage room with complex geometry has been simulated successfully with the present model, in which the interaction between the supply air and the stored products has been fully taken into consideration. It has been found that the structure of products strongly influences flow patterns inside the storage region. With a higher porosity or permeability, air flow inside the product is driven by the velocity generated by the air above it, and the air is circulated inside the product region. Provided a turbulent air flow is introduced, turbulence can be generated in the product region. However, for a product with low porosity or permeability, air penetrates from one side of the stack of products and flows out from the other side at a much lower velocity than the air above it.

REFERENCE

Antohe, B.V. & Lage, J.L. (1997) A general two-equation macroscopic turbulence model for incompressible flow in porous media. *Int. J. Heat Mass Trans.*, **40**, 3013–3024.

Beaver, G.S. & Joseph, D.D. (1967) Boundary conditions at a naturally permeable wall. *J. Fluid Mech.*, **13**, 197–207.

Beckermann, C., Viskanta, R. & Ramadhyani, S. (1988) Natural convection in vertical enclosures containing simultaneously fluid and porous layers. *J. Fluid Mech.*, **186**, 257–284.

Chen, F. & Chen, C.F. (1992) Convection in superposed fluid and porous layers. *J. Fluid Mech.*, **234**, 97–119.

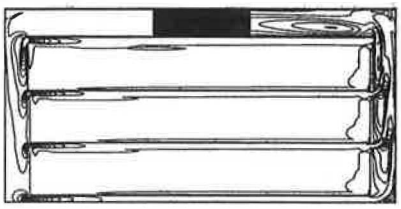

Figure 13 Turbulent kinetic energy contours for apples (levels: 0.001–8) for $d = 8 \times 10^{-2}$, $F = 0.4767$.

Fong, M. (1996) Gas flow behaviour in confined spaces with particular application to controlled atmosphere cool rooms, Master of engineering thesis, RMIT, Autralia.

Henkes, R.A.W.M., Van Der Vlugt, F.F. & Hoogendoorn, C.J. (1991) Natural-convection flow in a square cavity calculated with low-Reynolds-number turbulence model. *Int. J. Heat Mass Trans.*, **34**, 377–388.

Hsu, C.T. & Cheng, P. (1991) Thermal dispersion in a porous medium. *Int. J. Heat Mass Trans.*, **33**, 1587–1597.

Nield, D.A. (1991) The limitations of the Brinkman–Forchheimer equation in modelling flow in a saturated porous medium and at an interface. *Int. J. Heat Mass Trans.*, **12**, 269–272.

Ochoa–Tapia, J.A. & Whitaker, S. (1995) Momentum transfer at the boundary between a porous medium and a homogenous fluid – I. Theoretical development. *Int. J. Heat Mass Trans.*, **38**, 2635–2646.

Li, Y. & Rudman, M. (1995) Assessment of higher-order upwind schemes incorporating FCT for convection-dominated problems. *Num. Heat Trans., Part B*, **27**, 1–21.

Patankar, S.V. (1980) *Numerical Heat Transfer and Fluid Flow*. Hemisphere.

Song, M. & Viskanta, R. (1994) Natural convection flow and heat transfer within a rectangular enclosure containing a vertical porous layer. *Int. J. Heat Mass Trans.*, **37**, 2425–2438.

Tanka, A. & Xin, H. (1997) Effects of structural and stacking configuration on containers for transporting chicks in their microenvironment. *Tans. ASAE*, **40**(3), 777–782.

Vafai, K. & Kim, S.J. (1995) On the limitations of the Brinkman–Forchheimer-extended Darcy equation. *Int. J. Heat Fluid Flow*, **16**, 11–15.

Vafai, K. & Tien, C.L. (1981) Boundary and inertia effects on flow and heat transfer in porous media. *Int. J. Heat Mass Trans.*, **30**, 1391–1405.

Wang, H. & Touber, S. (1990) Distributed dynamic modelling of a refrigerated room. *Int. J. Refrig.* **13**, 214–222.